LA-UR- 09-00644

Approved for public release;
distribution is unlimited.

Title:	FLUCTUATIONS IN AN ELECTRON-POSITRON PLASMA: LINEAR THEORY AND IMPLICATIONS FOR TURBULENCE
Author(s):	S. Peter Gary, LANL/ISR-1 Homa Karimabadi, UCSD
Intended for:	Physics of Plasmas

Los Alamos
NATIONAL LABORATORY
EST. 1943

Form 836 (7/06)

Fluctuations in an electron-positron plasma: Linear theory and implications for turbulence

S. Peter Gary
Los Alamos National Laboratory
Los Alamos, NM 87545

Homa Karimabadi
Department of Electrical and Computer Engineering
University of California, San Diego
La Jolla, California 92093

29 January 2009

Abstract

Linear kinetic theory of electromagnetic fluctuations in a homogeneous, magnetized, collisionless electron-positron plasma predicts two lightly damped modes propagate at relatively long wavelengths: an Alfvén-like mode with dispersion $\omega_r = k_\parallel \tilde{v}_A$ and a magnetosonic-like mode with dispersion $\omega_r \simeq k\tilde{v}_A$ if $\beta_e << 1$. Here $\tilde{v}_A$ is the Alfvén speed in an electron-positron plasma and $\parallel$ refers to the direction relative to the background magnetic field $\mathbf{B}_o$. The Alfvén-like fluctuations are incompressible, but the magnetosonic-like fluctuations become compressible at propagation oblique to $\mathbf{B}_o$. The onset of cyclotron damping of both modes moves to smaller $k_\parallel c/\omega_e$ as $\beta_{\parallel e}$ increases. Using the linear dispersion properties of these modes, scaling relations are derived which predict that turbulence of both modes should be relatively anisotropic, with fluctuating magnetic energy preferentially cascading in directions relatively perpendicular to $\mathbf{B}_o$. But two-regime turbulence with a distinct breakpoint in wavenumber space observed in the solar wind should not be present in electron-positron plasmas because of the absence of whistler-like dispersion. Linear theory properties of the cyclotron and mirror instabilities driven by either electron or positron temperature anisotropies are generally analogous to the corresponding instabilities in electron-proton plasmas.

I. INTRODUCTION

It has been hypothesized that weak homogeneous turbulence in collisionless, magnetized plasmas reflects the properties of its constituent small-amplitude fluctuations. This hypothesis can be most directly tested through the use of particle-in-cell (PIC) simulations; however, current computing facilities do not yet allow long-time simulations of plasma turbulence with physically realistic proton-electron mass ratios. But substantial simulations

of turbulence in electron-positron plasmas do lie within the realm of current capability, so it is appropriate to use linear theory of electromagnetic fluctuations to predict basic properties of such turbulence. Thus electron-positron PIC models can be powerful tools for testing predictions drawn from fundamental theories of plasma turbulence and magnetic reconnection [*Bessho and Bhattacharjee*, 2007; *Daughton and Karimabadi*, 2007; *Drake et al.*, 2008; *Yin et al.*, 2008].

The first PIC simulation of whistler turbulence [*Gary et al.*, 2008] demonstrated the forward cascade of such fluctuations from relatively long to shorter wavelengths, and also showed that such turbulence becomes anisotropic with more energy at directions of propagation relatively perpendicular to the background magnetic field $\mathbf{B}_o$ as contrasted with directions relatively parallel to $\mathbf{B}_o$. *Saito et al.* [2008] carried out further PIC simulations of whistler turbulence, showing that the turbulence becomes more anisotropic as the fluctuation amplitudes increase, and deriving scaling arguments which predict an anisotropy consistent with that obtained from the computations.

As a preface for future possible PIC simulations of turbulence in magnetized collisionless electron-positron plasmas, we here consider the linear theory of fluctuations in such plasmas, and use the results to construct scaling relations analogous to those of *Saito et al.* (2008). If the electron and positron temperatures are similar, electrostatic fluctuations at frequencies below the plasma frequency are heavily damped in an electron-positron plasma, so we here address electromagnetic fluctuations. There are two distinct electromagnetic modes in an isotropic electron-positron plasmas, analogous to the Alfvén and magnetosonic modes of an electron-proton plasma; we label them the Alfvén-like and magnetosonic-like modes. Section II describes some of the linear theory properties of these two modes. Section III uses these linear properties to predict some properties of turbulence in an electron-positron plasma. Section IV describes linear theory properties of the cyclotron and mirror instabilities driven by temperature anisotropies on either the electrons or the positrons. Section V draws some conclusions from our research.

We denote the jth species plasma frequency as $\omega_j \equiv \sqrt{4\pi n_j e_j^2/m_j}$, the jth species cyclotron frequency as $\Omega_j \equiv e_j B_o/m_j c$, and $\beta_{\parallel j} \equiv 8\pi n_j k_B T_{\parallel j}/B_o^2$. Solutions to the linear dispersion equation are in terms of a wavevector $\mathbf{k}$ with real components and a complex frequency $\omega = \omega_r + i\gamma$. The symbols $\parallel$ and $\perp$ denote directions parallel and perpendicular, respectively, to the background magnetic field $\mathbf{B}_o$. Here the Alfvén speed in an electron-positron plasma is $\tilde{v}_A \equiv B_o/\sqrt{8\pi n_e m_e}$. We define θ, the angle of mode propagation, by $\mathbf{k} \cdot \mathbf{B}_o = kB_o \cos(\theta)$.

II. LINEAR THEORY

This section describes results from the solution of the linear kinetic dispersion equation for electromagnetic fluctuations in a homogeneous, collisionless electron-positron

plasma. Unless stated otherwise, the dimensionless parameters characterizing the zeroth order background plasma are $\beta_{\|e} = 0.10$, $\omega_e/|\Omega_e| = 2.5$, $T_e = T_p$, $T_{\perp j} = T_{\|j}$, and $m_e = m_p$ where the subscripts e and p refer to electron and positron, respectively. Our results are essentially independent of $\omega_e/|\Omega_e|$ as long as this parameter is much greater than unity. We choose $\omega_e/|\Omega_e| = 2.5$ for our calculations because PIC simulations run most efficiently when $\omega_e/|\Omega_e|$ is of order unity. We assume the zeroth order velocity distribution of each species is a Maxwellian or bi-Maxwellian, and solve the full electromagnetic dispersion equation [*Gary*, 1993] without analytic approximation.

Linear theory yields two distinct electromagnetic modes, which we call the Alfvén-like and magnetosonic-like modes, with linear dispersion properties illustrated in Figures 1 and 2. At $\mathbf{k} \times \mathbf{B}_o = 0$, the two modes have identical dispersion and damping, with $\omega_r = k\tilde{v}_A$ and essentially zero damping at $kc/\omega_e << 1$. At parallel propagation, the Alfvén-like mode is left-hand circularly polarized, and the magnetosonic-like mode is right-hand circularly polarized. At shorter wavelengths, the cyclotron resonances begin to assert themselves (positron cyclotron resonance for the Alfvén-like mode and the electron cyclotron resonance for the magnetosonic-like mode), ω_r becomes dispersive, and cyclotron damping displays its characteristic rapid onset as $k_\| c/\omega_e$ approaches unity.

At propagation oblique to $\mathbf{B}_o$, however, the properties of the two modes diverge; the Alfvén-like mode shown in Figure 1 satisfies $\omega_r = k_\| \tilde{v}_A$ at long wavelength, whereas the magnetosonic-like mode shown in Figure 2 is more nearly isotropic with $\omega_r \simeq k\tilde{v}_A$ at $kc/\omega_e << 1$. The Alfvén-like mode remains incompressible at oblique propagation; that is, both the magnetic compressibility

$$C_\| \equiv \frac{|\delta B_\||^2}{|\delta \mathbf{B}|^2}$$

and the jth species compressibility

$$C_j \equiv \frac{|\delta n_j|^2}{n_j^2} \frac{B_o^2}{|\delta \mathbf{B}|^2}$$

are zero for all wavenumbers and angles shown here. The Alfvén-like mode at oblique propagation is analogous to the kinetic Alfvén mode at $m_p = 1836 m_e$; not only are both incompressible, but both have a non-zero fluctuating electric field component parallel to $\mathbf{B}_o$. This is illustrated in Figure 1b, which shows that this quantity grows with increasing wavenumber and increasing θ. At oblique propagation the magnetosonic mode also displays a non-zero $|\delta E_\||^2/|\delta \mathbf{E}|^2$ and $C_\| = 0$; it differs from the Alfvén-like mode in that it has non-zero electron and positron compressibilities as shown in Figure 2b.

Figure 3 illustrates the $\beta_{\|e}$ dependence of dispersion and damping for the magnetosonic-like mode at parallel propagation. With increasing $\beta_{\|e}$, the mode show

stronger dispersion (i.e. $\omega_r < k_\| \tilde{v}_A$) at short wavelengths, and the onset of electron cyclotron damping takes place at smaller values of $k_\| c/\omega_e$. The same figure (not shown) applies to the Alfvén-like mode at $\mathbf{k} \times \mathbf{B}_o = 0$. As $\beta_{\|p}$ increases, the mode shows stronger dispersion and the onset of positron cyclotron damping arises at smaller values of $k_\| c/\omega_e$. At $\mathbf{k} \times \mathbf{B}_o = 0$ the magnetosonic-like mode is relatively independent of variations in $\beta_{\|p}$, and the Alfvén-like mode is similarly independent of variations in $\beta_{\|e}$.

III. SCALING RELATIONS

This section uses the results of Section II to construct a scenario for cascading turbulence in a homogeneous electron-positron plasma. Our two fundamental assumptions are, first, that linear dispersion and dissipation determine the characteristics of such weak turbulence [*Stawicki et al.*, 2001] and, second, that some nonlinear properties of the turbulence follow from arguments parallel to those applied to weak whistler turbulence [*Biskamp et al.*, 1996; *Galtier and Bhattacharjee*, 2003; *Cho and Lazarian*, 2004; *Saito et al.*, 2008].

Observations [*Smith et al.*, 2006] suggest that there are two distinct regimes of the solar wind turbulence cascade: the long-wavelength inertial range with $|\delta\mathbf{B}|^2 \sim k^{-\alpha}$ with $\alpha \simeq 5/3$, and a shorter wavelength regime with $\alpha > 5/3$ often termed the "dissipation range". The breakpoint between the two regimes lies approximately at $kc/\omega_{proton} \simeq 1$. *Stawicki et al.* [2001] attribute this breakpoint to the transition from Alfvén-like dispersion ($\omega_r \simeq kv_A$) at longer wavelengths to whistler-like dispersion ($\omega_r \sim k^2$) at shorter wavelengths. Linear theory yields no such transition in electron-positron plasmas. Thus we predict no breakpoint in homogeneous electron-positron turbulence; there should be only a relatively steep ($\alpha > 5/3$) power law spectrum in the cascade regime, followed by a true dissipation range with a faster-than-power-law spectral decrease at $kc/\omega_e > 1$ as predicted by *Li et al.* [2001].

Next, we consider the interaction of wave packets with parallel widths $l_\| = 2\pi/k_\|$ where the constituent modes each satisfy either the Alfvén-like dispersion equation $\omega_r \simeq k_\| \tilde{v}_A$ or the low-β magnetosonic-like $\omega_r \simeq k\tilde{v}_A$. The wave packet interaction time τ_w is determined by fluctuation properties at propagation parallel to $\mathbf{B}_o$, so

$$\tau_w \simeq \frac{l_\|}{(\partial\omega/\partial k_\|)} \tag{1}$$

For an eddy of scale length l the turnover time is $\tau_{eddy} \simeq l/\delta v_e$ where the denominator is the fluctuating electron velocity from the EMHD model. Then

$$\tau_{eddy} \simeq \frac{2\pi}{|\Omega_e|} \frac{\omega_e^2}{k^2c^2} \frac{B_o}{|\delta\mathbf{B}|} \tag{2}$$

Following the usual assumption of weak incoherent interactions between eddies, the time scale for the cascade of turbulent fluctuation energy is

$$\tau_{cascade} \equiv \frac{\tau_{eddy}^2}{\tau_w} \tag{3}$$

First consider Alfvén-like fluctuations with

$$\tau_w(k) \simeq \frac{2\pi}{k_\parallel \tilde{v}_A}$$

Then the cascade time is

$$\tau_{cascade}(k) \simeq \frac{2\pi}{|\Omega_e|} \frac{k_\parallel}{\sqrt{2}k} \frac{\omega_e^3}{k^3 c^3} \frac{B_o^2}{|\delta \mathbf{B}(k)|^2} \tag{4}$$

Second, consider interacting magnetosonic-like wave packets with

$$\tau_w(k) \simeq \frac{2\pi}{k_\parallel \tilde{v}_A} \frac{k}{k_\parallel}$$

and it follows that the cascade time is

$$\tau_{cascade}(k) \simeq \frac{2\pi}{|\Omega_e|} \frac{k_\parallel^2}{\sqrt{2}k^2} \frac{\omega_e^3}{k^3 c^3} \frac{B_o^2}{|\delta \mathbf{B}(k)|^2} \tag{5}$$

We consider two cases: Case I with $k_\perp >> k_\parallel$, and Case II with $k_\perp << k_\parallel$. We also make two assumptions: first, that the $k_\perp$ of Case I is of the same order as $k_\parallel$ of Case II, and, second, that $|\delta \mathbf{B}(k_\perp)|^2 \sim |\delta \mathbf{B}(k_\parallel)|^2$. Then for the Alfvén-like fluctuations it follows that

$$\frac{\tau_{cascade}(k_\perp)}{\tau_{cascade}(k_\parallel)} \simeq \left(\frac{k_\parallel}{k_\perp}\right)_I << 1$$

Similarly, for magnetosonic-like fluctuations, we have

$$\frac{\tau_{cascade}(k_\perp)}{\tau_{cascade}(k_\parallel)} \simeq \left(\frac{k_\parallel}{k_\perp}\right)_I^2 <<< 1$$

This model therefore implies that, for both modes, the cascade of magnetic fluctuation energy is much faster in directions quasi-perpependicular to $\mathbf{B}_o$ than in directions quasi-parallel to the background field. We thus predict that the cascade regime of electron-positron turbulence should display the same type of anisotropy as found in PIC simulations of cascading whistler turbulence [*Gary et al.*, 2008; *Saito et al.*, 2008]. But for fluctuations at similar wavenumbers, the model further implies that the ratio of the perp-versus-parallel cascade rates are much faster for the magnetosonic-like fluctuations, implying that magneotsonic-like turbulence should be more anisotropic than Alfvén-like turbulence.

IV. INSTABILITIES

In this section, we return to linear theory to consider the consequences of the temperature anisotropy $T_{\perp j}/T_{\|j} > 1$ separately on the positrons and electrons. In an electron-proton plasma, this anisotropy on the protons leads to two distinct instabilities, the Alfvén-cyclotron instability with $0 < \omega_r < \Omega_{proton}$ and maximum growth rate at $\mathbf{k} \times \mathbf{B}_o = 0$ and the proton mirror instability with $\omega_r = 0$ in a homogeneous plasma and which grows only at propagation oblique to the background magnetic field. If $\beta_{proton} \sim 1$, these two modes have similar growth rates and threshold anisotropy conditions [*Gary et al.*, 1993]. On the other hand, if $T_{\perp e}/T_{\|e} > 1$, the whistler anisotropy instability at $\Omega_{proton} < \omega_r < |\Omega_e|$ and maximum growth at $\mathbf{k} \times \mathbf{B}_o = 0$ has a far larger growth rate than the electron-driven mirror if $m_p >> m_e$.

In an electron-positron plasma $T_{\perp e}/T_{\|e} > 1$ can drive the magnetosonic-like mode unstable, just as a sufficiently large $T_{\perp p}/T_{\|p} > 1$ will lead to instability of the Alfvén-like mode. The relevant wave-particle interactions here are the cyclotron resonances, so we name these two growing modes the electron cyclotron and positron cyclotron instabilities, respectively. Figure 4 shows the dispersion of the electron cyclotron instability at three angles of propagation. By analogy with the whistler anisotropy instability, the maximum growth rate γ_m is at $\mathbf{k} \times \mathbf{B}_o = 0$ and $k_\| c/\omega_e \simeq 1$. For the same parameters except isotropic electrons and $T_{\perp p}/T_{\|p} = 3.0$, the positron cyclotron instability has identical dispersion properties. For both instabilities, $\gamma/|\Omega_j|$ increases with increasing species anisotropy and increasing $\beta_{\|j}$.

In addition to the relatively incompressible cyclotron instabilities with maximum growth at $\mathbf{k} \times \mathbf{B}_o = 0$, a $T_\perp/T_\|$ which is sufficiently greater than unity can also drive a compressible mirror instability with maximum growth highly oblique to $\mathbf{B}_o$. Figure 5 illustrates some dispersion properties of the positron mirror instability for a single choice of plasma parameters. The maximum growth rate lies at a wavevector strongly oblique (but not strictly perpendicular) to $\mathbf{B}_o$; increasing the anisotropy pushes γ_m to smaller values of θ. The positron compressibility is nonzero but relatively small; although C_e is not shown, $C_e \lesssim C_p$ for the parameters shown here. In contrast, Figure 5b shows that the magnetic compressibility is close to unity. Each of these properties is similar to those of the proton mirror instability in an electron-proton plasma. Sample computations show that, if the only change in the parameters is to transfer the positron anisotropy to the electrons, the growth rate of the electron mirror instability has exactly the same wavevector dependence as that of the positron anisotropy instability.

Figure 6 shows the threshold anisotropies at three different values of the maximum growth rate for the positron mirror instability (dotted lines) and the positron cyclotron instability (solid and dashed lines) as functions of $\beta_{\|p}$. The results are qualitatively similar to the thresholds for the analogous Alfvén-cyclotron and proton mirror instabilities in an

electron-proton plasma [*Gary et al.*, 1993]; at $\beta_{\|p} \lesssim 5$ the positron cyclotron instability has the smaller threshold anisotropy, whereas the positron mirror instability has the lower threshold if $\beta_{\|p}$ is sufficiently large and $\gamma_m/\Omega_p \leq 0.01$. However, in contrast to the electron-proton case, Figure 6 shows that, if the maximum growth rate is sufficiently large, the positron cyclotron instability has the lower threshold anisotropy over $1 \leq \beta_{\|p} \leq 100$.

V. CONCLUSIONS

We have used linear kinetic dispersion theory to study electromagnetic fluctuations in a magnetized, homogeneous, collisionless electron-positron plasma. There are two weakly damped electromagnetic modes: the incompressible Alfvén-like fluctuation and the magnetosonic-like fluctuation which becomes compressible at propagation oblique to the background magnetic field. The two modes have identical dispersion and damping at $\mathbf{k} \times \mathbf{B}_o = 0$, where the onset of cyclotron damping arises near $k_\| c/\omega_e \simeq 1$. A sufficiently large $T_{\perp e}/T_{\|e}$ drives the electron cyclotron instability while a sufficiently large $T_{\perp p}/T_{\|p}$ excites the positron cyclotron instability with maximum growth rate in both cases at $\mathbf{k} \times \mathbf{B}_o = 0$ and $k_\| c/\omega_j \simeq 1$. The same anisotropies can also excite the electron mirror and positron mirror instabilities with maximum growth rate at propagation oblique to $\mathbf{B}_o$ and $kc/\omega_e < 1$.

Using our linear theory results and a basic turbulence model, we have made predictions concerning properties of homogeneous turbulence in electron-positron plasmas which can be tested by future particle-in-cell simulations. We predict that cascading turbulence will be anisotropic in the same sense as MHD and whistler turbulence. However, in the absence of whistler-like dispersion, we further predict that there will be only a single regime of turbulent cascade with power-law spectra, followed by a true dissipation range of rapidly decreasing spectra at $kc/\omega_e \gtrsim 1$. These predictions now can be tested with PIC simulations in an electron-positron plasma model, while awaiting improvements in computing power and speed that will permit full-fledged PIC simulations of turbulence in electron-proton plasmas at some later date.

If these predictions are confirmed by PIC simulations in $m_p = m_e$ plasmas, the next step should be to extend the simulations to the range $1 < m_p/m_e \leq 1836$. At $m_p/m_e \simeq 64$, linear theory predicts that the characteristic $\omega_r \sim k_\| k$ dispersion of the whistler emerges on the magnetosonic-like mode. Thus, PIC simulations of turbulence at $m_p/m_e \geq 64$ should, if the hypothesis of *Stawicki et al.* (2001) is correct, then yield cascading spectra with two distinct power law regimes separated by a breakpoint at $kc/\omega_{proton} \sim 1$. Such computations would also help resolve the current controversy as to whether short wavelength turbulence observed in the solar wind is primarily due to whistler modes at $\omega_r > \Omega_{proton}$ [*Saito et al.*, 2008] or to kinetic Alfvén fluctuations at $\omega_r < \Omega_{proton}$ [*Leamon et al.*, 1998].

Acknowledgments. The Los Alamos portion of this work was performed under the aus-

pices of the U.S. Department of Energy (DOE). It was supported by by the Magnetic Turbulence and Kinetic Dissipation Project of the Laboratory Directed Research and Development Program at Los Alamos, and by the Solar and Heliospheric Physics SR&T Program of the National Aeronautics and Space Administration.

References

Bessho, N., and A. Bhattacharjee (2007), Fast collisionless reconnection in electron-positron plasmas, *Phys. Plasmas*, *14*, 056503.

Biskamp, D., E. Schwartz, and J. F. Drake (1996), *Phys. Rev. Lett.*, *76*, 1264.

Cho, J., and A. Lazarian (2004), *Astrophys. J.*, *615*, L41.

Daughton, W., and H. Karimabadi (2007), Collisionless magnetic reconnection in large-scale electron-positron plasmas, *Phys. Plasmas*, *14*, 072303.

Drake, J. F., M. A. Shay, and M. Swisdak (2008), The Hall fields and fast magnetic reconnection, *Phys. Plasmas*, *15*, 042306.

Galtier, S., and A. Bhattacharjee (2003), *Phys. Plasmas*, *10*, 3065.

Gary, S. P. (1993), *Theory of Space Plasma Microinstabilities*, Cambridge University Press, New York.

Gary, S. P., S. A. Fuselier, and B. J. Anderson (1993), Ion anisotropy instabilities in the magnetosheath, *J. Geophys. Res.*, **98**, 1481.

Gary, S. P., S. Saito, and H. Li (2008), Cascade of whistler turbulence: Particle-in-cell simulations, *Geophys. Res. Lett.*, *35*, L02104, doi:10.1029/2007GL032327.

Leamon, R. J., C. W. Smith, N. F. Ness, W. H. Matthaeus, and H. K. Wong (1998), *J. Geophys. Res.*, **103**, 4775.

Li, H., S. P. Gary, and O. Stawicki (2001), On the dissipation of magnetic fluctuations in the solar wind, *Geophys. Res. Lett.*, *28*, 1347.

Saito, S., S. P. Gary, H. Li, and Y. Narita (2008), Whistler turbulence: Particle-in-cell simulations, *Phys. Plasmas*, **15**, 102305.

Stawicki, O., S. P. Gary, and H. Li (2001), Solar wind magnetic fluctuation spectra: Dispersion versus damping, *J. Geophys. Res.*, *106*, 8273.

Yin, L., W. Daughton, B. J. Albright, K. J. Bowers, J. Margulies (2008), Three-dimensional dynamics of collisionless magnetic reconnection in large-scale pair plasmas, *Phys. Rev. Lett.*, *101*, 125001.

Figure Captions

Figure 1. Linear dispersion properties of the Alfvén-like mode in an electron-positron plasma with parameters as stated in Section II. (a) The real frequency $\omega_r/|\Omega_e|$ and the damping rate $\gamma/|\Omega_e|$ as functions of wavenumber k for angles of propagation as

labeled. (b) The dimensionless parameter $|\delta E_\parallel|^2/|\delta \mathbf{E}|^2$ as a function of wavenumber k for angles of propagation as labeled.

Figure 2. Linear dispersion properties of the magnetosonic-like mode in an electron-positron plasma with parameters as stated in Section II. (a) The real frequency $\omega_r/|\Omega_e|$ and the damping rate $\gamma/|\Omega_e|$ as functions of wavenumber k for angles of propagation as labeled. (b) The electron compressibility C_e as functions of wavenumber k for angles of propagation as labeled.

Figure 3. Linear dispersion properties at $\mathbf{k} \times \mathbf{B}_o = 0$ of the magnetosonic-like mode in an electron-positron plasma. Except for $\beta_{\parallel e}$, parameters are as stated in Section II. Here the real frequency $\omega_r/|\Omega_e|$ and the damping rate $\gamma/|\Omega_e|$ are shown as functions of wavenumber $k_\parallel$ with $\beta_{\parallel e} = 0.10$ and 1.00 as labeled.

Figure 4. Linear dispersion properties of the electron cyclotron instability with $T_{\perp e}/T_{\parallel e} = 3.0$ in an electron-positron plasma. All other parameters are as stated in Section II. The real frequency $\omega_r/|\Omega_e|$ and the growth/damping rate $\gamma/|\Omega_e|$ are shown as functions of the wavenumber for angles of propagation as labeled. At $\theta = 0^o$, the results are identical for the positron cyclotron instability with $T_{\perp p}/T_{\parallel p} = 3.0$.

Figure 5. Linear dispersion properties of the positron mirror instability as functions of the direction of propagation in an electron-positron plasma. Panel (a) shows the growth rate and the positron compressibility, whereas panel (b) shows the magnetic compressibility as functions of θ. Parameters are as stated in Section II and as given in panel (b).

Figure 6. Threshold positron anisotropies as functions of $\beta_{\parallel p}$ for three different values of the maximum growth rate of the positron cyclotron instability (solid and dashed lines) and the positron mirror instability (dotted lines). Other parameters are as stated in Section II.

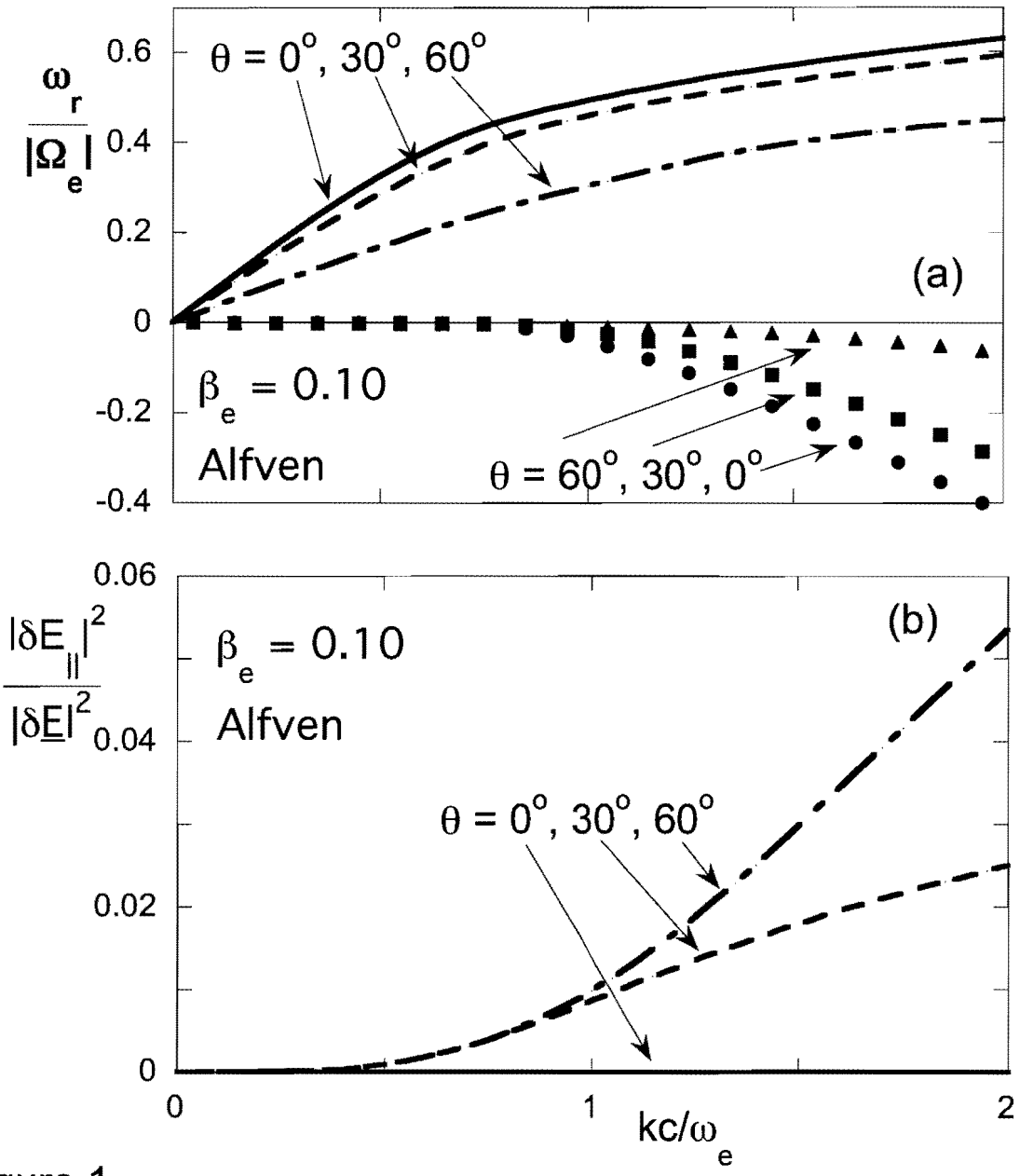
$\frac{\omega_r}{|\Omega_e|}$
0.6
0.4
0.2
0
-0.2
-0.4
θ = 0°, 30°, 60°
(a)
β_e = 0.10
Alfven
θ = 60°, 30°, 0°
$\frac{|\delta E_{\parallel}|^2}{|\delta \underline{E}|^2}$
0.06
0.04
0.02
0
(b)
β_e = 0.10
Alfven
θ = 0°, 30°, 60°
0
1
2
kc/ω_e

Figure 1

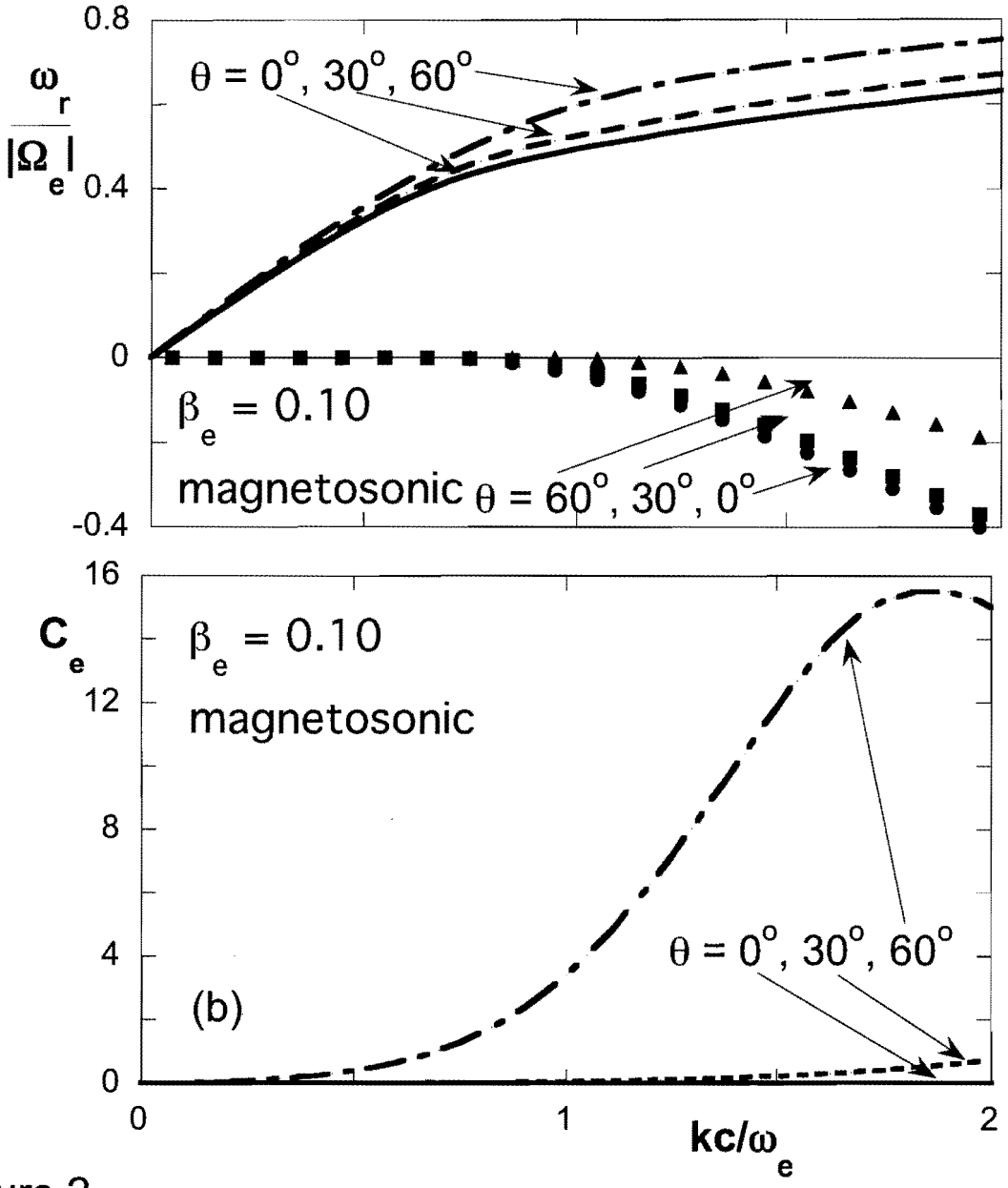
0.8
$\frac{\omega_r}{|\Omega_e|}$
0.4
0
-0.4
θ = 0°, 30°, 60°
β_e = 0.10
magnetosonic
θ = 60°, 30°, 0°
16
C_e
12
8
4
0
β_e = 0.10
magnetosonic
(b)
θ = 0°, 30°, 60°
0
1
2
kc/ω_e

Figure 2

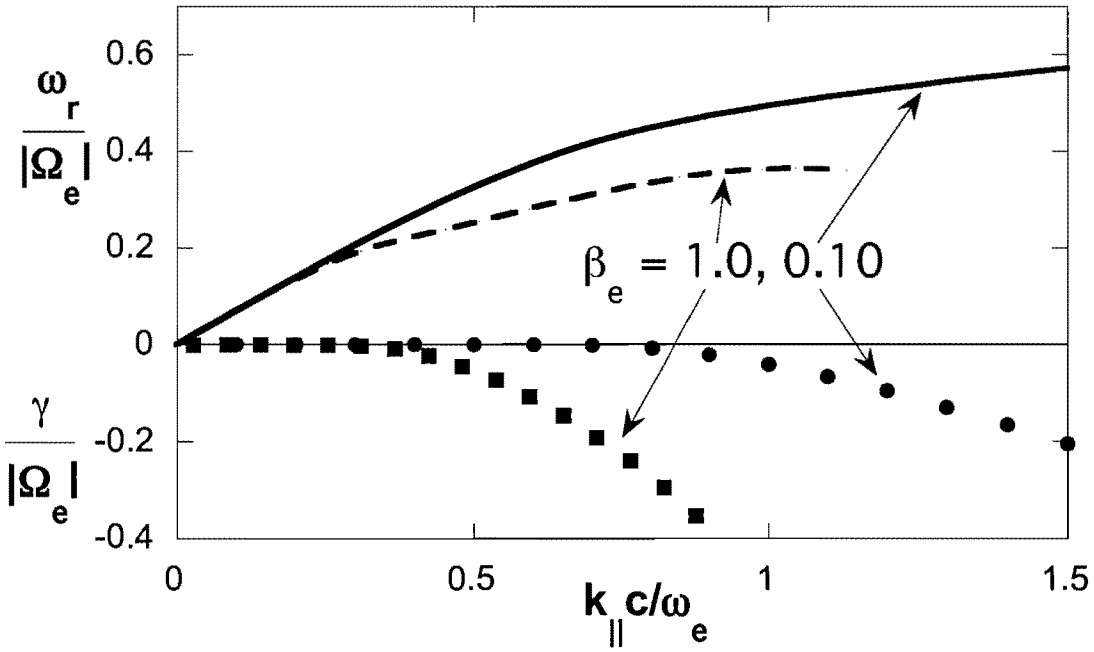

Figure 3

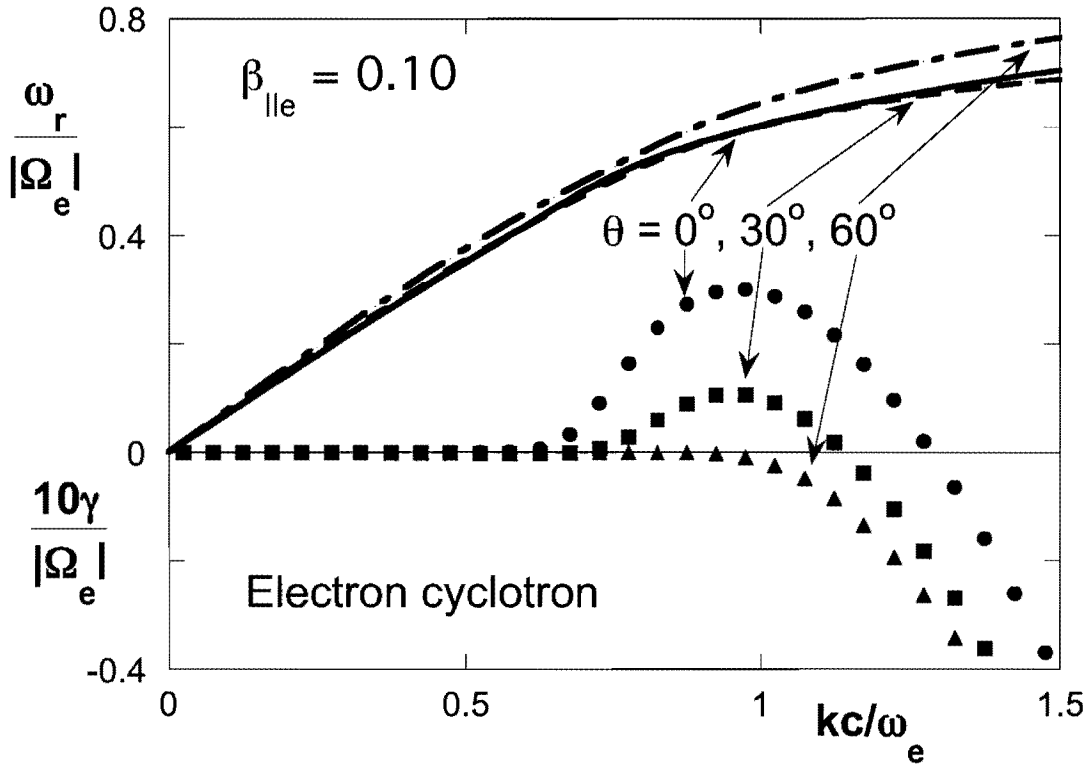
0.8
0.4
0
-0.4
$\frac{\omega_r}{|\Omega_e|}$
$\frac{10\gamma}{|\Omega_e|}$
$\beta_{\|e} = 0.10$
$\theta = 0^o, 30^o, 60^o$
Electron cyclotron
0
0.5
1
1.5
kc/ω_e

Figure 4

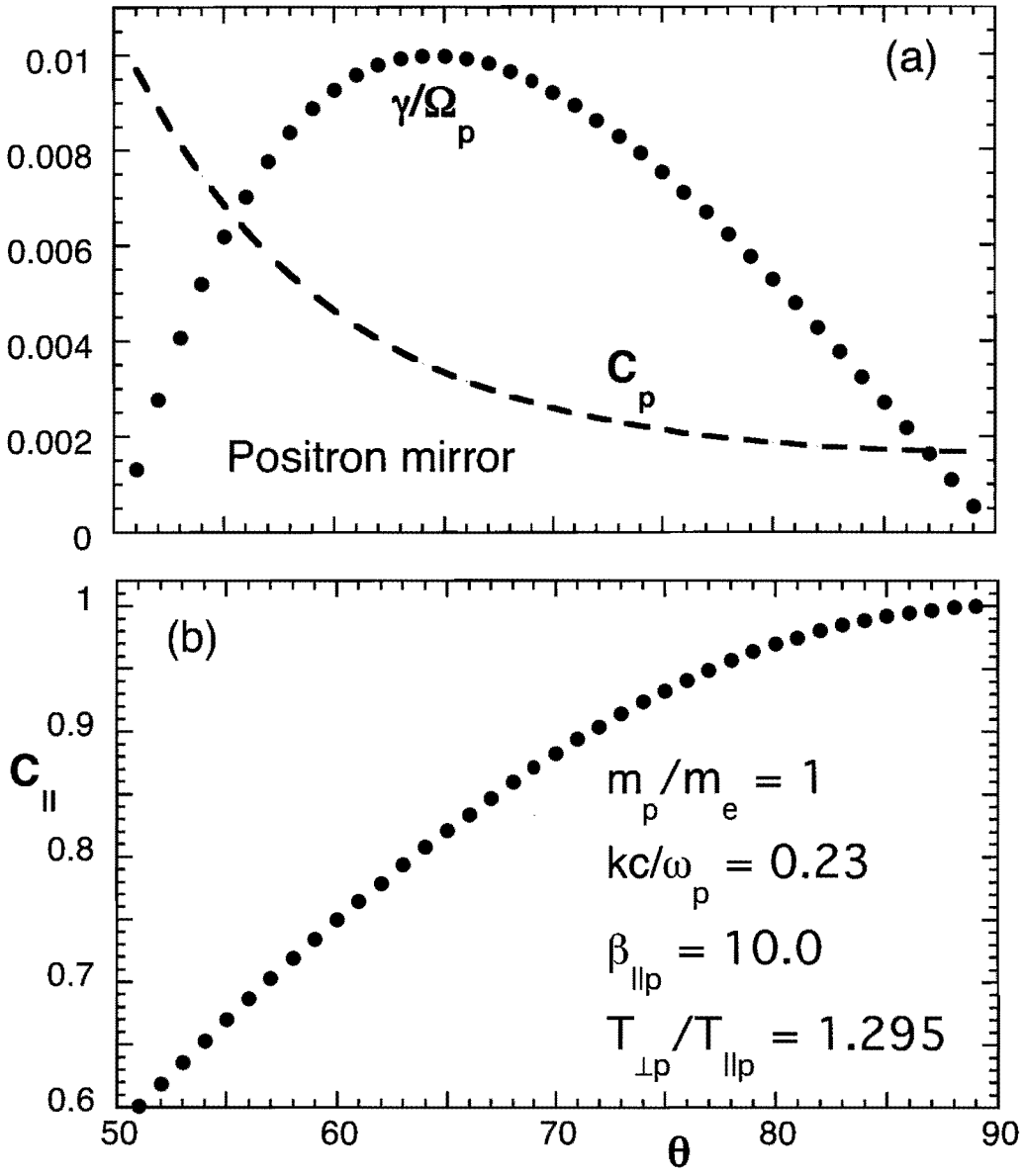
(a)
γ/Ω_p
c_p
Positron mirror
0.01
0.008
0.006
0.004
0.002
0
(b)
c_||
m_p/m_e = 1
kc/ω_p = 0.23
β_||p = 10.0
T_⊥p/T_||p = 1.295
1
0.9
0.8
0.7
0.6
50
60
70
80
90
θ

Figure 5

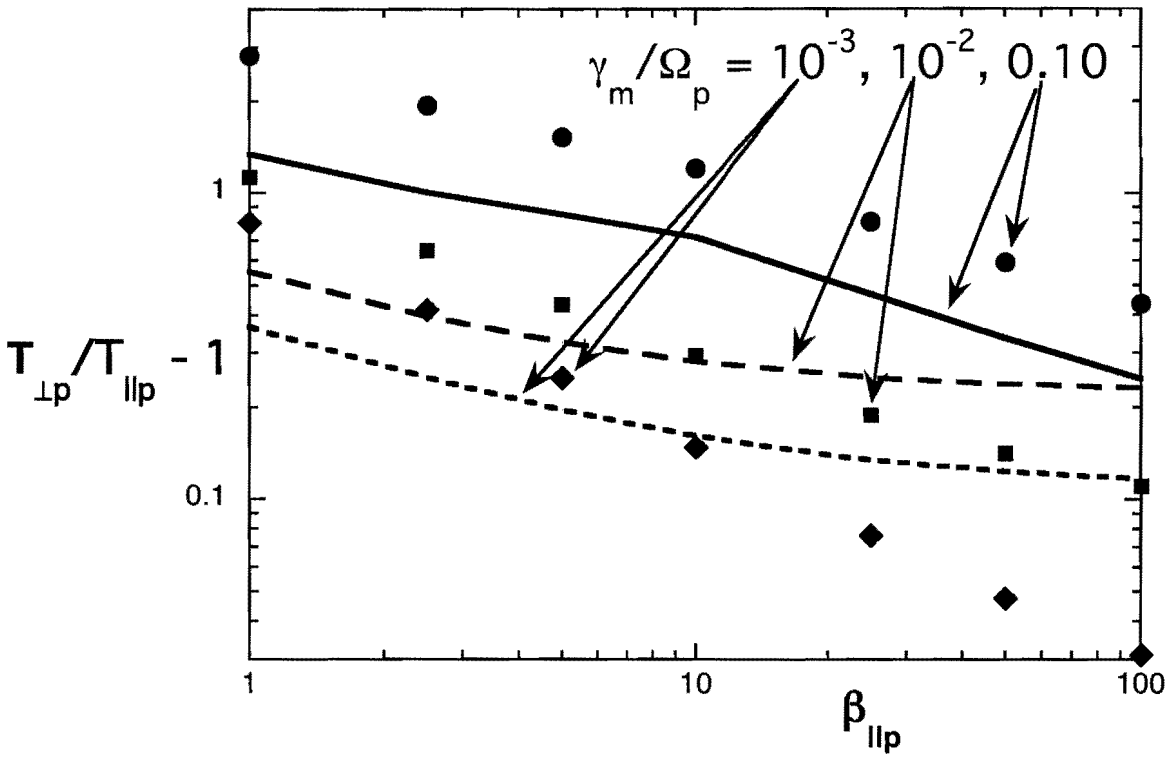
$\gamma_m/\Omega_p = 10^{-3}, 10^{-2}, 0.10$
$T_{\perp p}/T_{\parallel p} - 1$
1
0.1
1
10
100
$\beta_{\parallel p}$

Figure 6